ON MODELING THE MECHANICAL BEHAVIOR AND TEXTURE EVOLUTION OF ROLLED AZ31 MG FOR COMPLEX LOADINGS INVOLVING STRAIN PATH CHANGES

NITIN CHANDOLA[1], CRYSTAL PASILIAO[2],
OANA CAZACU[1], BENOIT REVIL-BAUDARD[1]

Abstract. An accurate description of the deformation response of AZ31 Mg under changing strain paths requires consideration of its strong anisotropy and its evolution with accumulated plastic deformation. In this paper, the viscoplastic self-consistent mean field crystal plasticity model, VPSC, is used for modeling the room-temperature deformation of rolled AZ31 Mg for a variety of loading paths. First, a step-by-step procedure, to calibrate the material parameters based on simple monotonic tensile and compressive mechanical test data is outlined. The good agreement between measured and predicted textures for these strain paths attest to the robustness of the identification. Next, it is investigated whether with the same set of parameters it is possible to predict the response of a thinner AZ31 Mg sheet. Specifically, it is shown that the model can predict with accuracy the macroscopic stress-strain response and texture evolution for loadings involving stress path changes. The interplay between slip and twinning and its influence on work hardening are well described.

Key words: AZ31 Mg, visco-plastic self consistent model, stress-path changes, texture evolution.

1. INTRODUCTION

There is a large body of literature devoted to the identification of the plastic deformation mechanisms operational in rolled Mg and its alloy AZ31 in plate and sheet form at room temperature under quasi-static loading conditions (e.g. [1–3]). The main conclusion of these investigations is that even for the simplest monotonic loadings because of twinning activity the mechanical response is very complex. Experimental data reported include the macroscopic stress-strain response and the microstructure evolution under uniaxial tension and compression along different

[1] University of Florida, Dept. of Mechanical and Aerospace Engineering, REEF,1350 N. Poquito Road Shalimar, FL 32579, USA.
[2] Air Force Research Laboratory, Eglin, FL 32542, USA.

orientations (see [2–4]), simple shear ([2, 3]), biaxial tension [5], etc. In comparison, there is little information concerning the mechanical behaviour of Mg and its alloys in torsion. Free-end torsion tests at room temperature, 150°C, and 250°C on solid bars of pure Mg and Mg alloy AZ71 with the axis along the rolling direction were reported (see in [6, 7]). The Swift phenomenon, which refers to the occurrence of plastic axial strains in free-end torsion, was observed. Specifically, for all temperatures, shortening of the specimens was reported. Very recently, in [8] were reported room-temperature torsion tests on AZ31 Mg alloy cylindrical solid bars machined from a rolled plate with a very strong initial basal texture. Specimens with longitudinal axis oriented along either the rolling direction, or the through-thickness (normal direction) direction of the plate were tested. It was found that while the sample with longitudinal axis along the rolling direction contracts, the sample with longitudinal axis along the normal direction elongates. The occurrence of axial strains under torsion was attributed to tensile twinning, which, in turn, induces texture evolution in the material. However, for hexagonal close packed (hcp) titanium with basal texture, elongation of the specimens is observed irrespective of the orientation of the long axis of the specimen as evidenced by the analysis of tubes obtained by flow-forming (see [9]).

In view of industrial applications (e.g. detailed finite-element (FE) analyses of complex forming processes), a robust macroscopic level analytical elastic/plastic model may be very useful. For materials with cubic crystal structure, models based on orthotropic yield functions that capture with very good accuracy both the anisotropy in flow stresses and Lankford coefficients have been developed (e.g. [10–14]). However, these models do not account for the experimentally observed very strong difference between the mechanical response in tension and compression observed in hcp materials.

In the last decade, models for hcp materials have been developed in the framework of the mathematical theory of plasticity. For example, using results of monotonic uniaxial tests and virtual experiments conducted using a self-consistent theory based plasticity model, orthotropic yield functions that account for both the anisotropy and tension-compression asymmetry of hcp materials have been proposed (see [15–17]). Furthermore, to account for evolving anisotropy in magnesium alloys subject to monotonic loadings, Graff *et al*. [18] used the yield function developed by Cazacu and Barlat [11] in conjunction with a direction-dependent hardening model.

Very recently, a new interpretation of the Swift phenomenon in isotropic materials was provided in [19] for monotonic torsion and in [20] for cyclic torsion using a macroscopic modelling framework. Using the isotropic form of Cazacu et al. [16] criterion, it was demonstrated analytically that the occurrence of axial strains in isotropic materials is related to a slight difference between the uniaxial yield in tension and compression of the given material. For initially anisotropic hcp materials (e.g. Ti and Mg alloys), in [21] it was shown that the orthotropic form of

Cazacu *et al*. [16] criterion in conjunction with isotropic hardening explains and predicts the nature (elongation or contraction) of the axial strains that develop in free-end torsion. More specifically, if for a given direction the material has the uniaxial yield stress in tension larger than that in compression, the specimen will contract when twisted along that direction, while, if the yield stress in uniaxial compression is larger than that in uniaxial tension, it will elongate. Furthermore, in [22] it was demonstrated that only by accounting for the combined effects of anisotropy and tension-compression asymmetry at polycrystal level, it is possible to explain and accurately predict the room-temperature torsional response of an AZ31 Mg material. This was shown by using two modelling approaches, namely: a viscoplastic self-consistent (VPSC) polycrystal model and a macroscopic plasticity model based on Cazacu *et al*. [16] criterion. Unlike Hill's criterion (see [6]), the Cazacu et al. [16] criterion quantitatively predicts the experimental results, namely: that the sample with axial direction along the rolling direction contracts, while the sample with axial direction along the normal direction elongates. Moreover, it was demonstrated that these experimentally observed axial strain effects can be quantitatively predicted with the VPSC polycrystal model, only if both slip and twinning are considered operational at single crystal level. On the other hand, if it is assumed that the plastic deformation is fully accommodated by crystallographic slip, the axial strains predicted by VPSC are very close with that predicted with Hill's criterion [6], which largely underestimates the measured axial strain in the rolling direction, and predicts zero axial strain in the normal direction.

By performing sequential tests involving load reversal, [3] revealed the effects of twinning and de-twining on the response of AZ31 Mg. The specificities of the plastic response of AZ31 Mg under cyclic loadings were recently modelled in [23].

The behaviour under strain path changes, in particular the marked difference in response under cyclic loading depending whether tension or compression is applied first were experimentally investigated in [3], and most recently in [24–26]. The volume fraction of twins observed during each stage of loading was measured either by acoustic emission, and/or metallographic measurements. The very unusual work-hardening behaviour observed in AZ31 Mg sheets was attributed to twinning and de-twinning.

Four different approaches have been developed in order to model twinning in the framework of crystal plasticity: the predominant twin reorientation (PTR) scheme (see [27]), the volume fraction transfer method (see [28]), the so-called Lagrangian approach (see [29]), and the composite-grain scheme [30]. To model both twinning and de-twinning mechanisms that are observed in cyclic loadings, a new physics-based model was developed in [24]. All these methods have been used in conjunction with either Taylor type [31, 32] or self-consistent homogenization methods (e.g. the VPSC model of Lebensohn and Tomé (see [33]) or the the EVPSC model of [34]).

Agnew and collaborators (e.g. [4,35]) have calibrated the VPSC model using as input the initial texture and uniaxial tension and compression stress-strain curves in the rolling direction (RD) and further used the VPSC model to demonstrate the importance of the <c+a> slip (also referred to as cross-slip) on texture evolution for uniaxial compression along the normal direction (ND) of the sheet. Choi et al. [36] identified the VPSC model parameters using the uniaxial curves along the in-plane axes of symmetry (RD and transverse direction (TD)) and further simulated the microstructure evolution for the same uniaxial strain paths. The capabilities of the VPSC model to describe the stress-strain response of AZ31 Mg for uniaxial tension and compression along the orthotropy axes RD and TD, and for uniaxial compression along ND were demonstrated by Wang *et al*. [37].

However, there is a large scatter in the values of the VPSC material parameters for AZ31 Mg reported by different authors. Also, there is a discrepancy between investigators as to which systems need to be operational in order to accommodate the applied strain for a given strain path. For example, Walde and Reidel [38] considered only three deformation systems active in uniaxial loadings, while Jain and Agnew [35] and Wang *et al*. [37] considered four deformation systems (three slip modes and tensile twinning) to be operational. A step-by-step procedure for identification of the VPSC parameters for an AZ31 Mg rolled sheet was proposed in [39]. It was shown that using the respective set of parameters, it is possible to describe the behaviour of AZ31 Mg for loading paths that were not used for calibration, such as off-axis uniaxial loadings, and simple shear loadings.

Recently, starting from the lamellar grain model of Lebensohn [40], Tomé and Kaschner [41] and Proust *et al*. (see [42]) developed a new description of twinning that accounts for twin shape and twin-parent interaction and further applied it to Zr. In order to address the role of twinning during strain path changes in AZ31 Mg, the latter model was further extended in [30] to incorporate de-twinning, and then implemented in the VPSC code. Very recently, the behaviour of AZ31 Mg during cyclic loadings was also modelled by Hama and collaborators [43] using a crystal plasticity finite-element (CPFE) framework.

In this paper, we show that by accounting for the reorientation of microstructure, associated with deformation twinning, it is possible to describe the mechanical response under strain path changes in AZ31 Mg. The outline of the paper is as follows. In Section 2, we briefly present the VPSC model and PTR scheme that will be used for modelling AZ31 Mg behaviour. Section 3 presents the identification of the VPSC model parameters for AZ31 Mg based on a few monotonic uniaxial tension and compression tests on a rolled sheet. The mechanical data and observed textures that are used for identification and comparison were reported in [2]. The good agreement between measured and predicted textures for these strain paths attest to the robustness of the identification. Next, it is investigated whether with the same set of parameters it is possible to predict the mechanical response of a thinner AZ31 sheet with similar initial texture

for which experimental results were reported by Hama and collaborators (see [25, 26]). Specifically, it is shown that the VPSC model in conjunction with the PTR scheme can predict with accuracy the macroscopic stress-strain response and texture evolution for loadings involving stress path changes. The interplay between slip and twinning and its influence on work hardening are well described. The predicted texture evolution for the given loadings are also shown (Section 4). A summary of the main findings is given in Section 5.

2. POLYCRYSTAL VPSC MODEL

The VPSC model will be used to gain understanding into the role of specific single crystal plastic deformation mechanisms on the macroscopic response of AZ31 Mg. A brief presentation of this polycrystalline model is presented in what follows while for a more detailed description the reader is referred to the review article [44].

In the model, the polycrystal is represented by a finite set of orientations, each one representing a given volume fraction chosen to reproduce the initial texture. The total deformation of the polycrystal is obtained by imposing successive strain increments and calculating the resulting shears in the active deformation systems in the constituent grains. A self-consistent approach is used to model the interaction of a grain with its surroundings. Each grain is treated as an anisotropic, viscoplastic, ellipsoidal inclusion embedded in a uniform matrix having the unknown properties (to be determined) of the polycrystal. Elastic deformations are neglected. Each deformation system (s) is characterized by a vector $\mathbf{n}^s$ (normal to the slip or twinning plane) and a vector $\mathbf{b}^s$ (Burgers vector or twinning shear direction). The local constitutive behaviour (i.e. the behaviour at the grain level) is considered to be:

$$\mathbf{d} = \sum_s \mathbf{m}^s \, \dot{\gamma}^s = \dot{\gamma}_0 \sum_s \mathbf{m}^s \left(\frac{\mathbf{m}^s : \boldsymbol{\sigma}}{\tau_c^s} \right)^n , \tag{1}$$

where $\mathbf{d}$ and $\boldsymbol{\sigma}$ are the strain rate and Cauchy stress in the grain. Eq. (1) expresses that the deformation rate $\mathbf{d}$ is given by the sum over all the shear rates contributed by all systems. The activation criterion (for both for slip and twinning) is given by the expression in parenthesis. In Eq. (1), $\mathbf{m}^s = (1/2)\left(\mathbf{b}^s \otimes \mathbf{n}^s + \mathbf{n}^s \otimes \mathbf{b}^s\right)$ and $\dot{\gamma}^s$ are the Schmid tensor, and the shear rate on the system (s), $\dot{\gamma}_0$ is a reference shear rate and n is parameter that accounts for strain-rate sensitivity. The symbol $\otimes$ denotes the dyadic product between any two vectors. The activity on each deformation system (s) increases when the resolved shear on that system (given by

$\mathbf{m}^s : \boldsymbol{\sigma}$) approaches a threshold value denoted as τ_c^s. The symbol: stands for the scalar product between any two second-order tensors **A** and **B**, i.e. $\mathbf{A} : \mathbf{B} = A_{ij} B_{ij}$, $i, j = 1 \ldots 3$. A Voce-type strain hardening law is considered, i.e. the threshold stress τ_c^s is allowed to increase in a time interval Δt according to:

$$\tau_c^s = \tau_0^s + \left(\tau_1^s + \theta_1^s \Gamma\right)\left(1 - \exp\left(-\frac{\theta_0^s \Gamma}{\tau_1^s}\right)\right), \tag{2}$$

where τ_0^s, τ_1^s, θ_0^s and θ_1^s are constants, and $\Gamma = \sum_s \dot{\gamma}^s \Delta t$ is the accumulated shear of all deformation systems. In addition, it is possible to incorporate self and latent hardening. More specifically, the increase in the threshold stress is calculated as:

$$\Delta \tau_c^s = \frac{\mathrm{d}\tau_c^s}{\mathrm{d}\Gamma} \sum h^{ss'} \dot{\gamma}^{s'} \Delta t \,, \tag{3}$$

where, the coefficients $h^{ss'}$ empirically account for the obstacles that new dislocations (or twins) associated with system s' create for the propagation of dislocations (or twins) on system s. Following the approach proposed by Van Houtte [27], twinning is treated as a pseudo-slip mechanism. Specifically, it differs from slip in its directionality, which means that activation of twinning is allowed only if the resolved shear stress is positive. As already mentioned, in the original implementation of VPSC [33], the twinning contribution to texture development is accounted for by means of the PTR scheme (see [28]). In this scheme, within each grain the shear strain contributed by each twin system and the associated volume fraction in the grain are tracked. The sum over all the twin systems associated with a given twin mode and over all grains, represents the "accumulated twin fraction", in the aggregate for the particular mode. The accumulated twin fraction for the aggregate, $V^{\mathrm{acc,mode}}$ is calculated as,

$$V^{\mathrm{acc,mode}} = \sum_g \sum_t \gamma^{g,t} \big/ S^t \,, \tag{4}$$

where, S^t (characteristic twin shear for the twinning mode) is a material parameter. Since it is not numerically feasible to consider each twinned fraction as a new orientation, a statistical approach is used to determine new orientations (for more details, see [33]). At each incremental step, grains are fully re-oriented provided that certain conditions are fulfilled. Specifically, an effective twinned fraction $V^{\mathrm{eff,mode}}$ associated with the fully reoriented grains for the given mode as well as a

threshold value $V^{\text{th,mode}}$ are defined. The threshold volume fraction $V^{\text{th,mode}}$ is defined as:

$$V^{\text{th,mode}} = A^{\text{th1}} + A^{\text{th2}} \frac{V^{\text{eff,mode}}}{V^{\text{acc,mode}}}, \tag{5}$$

where A^{th1} and A^{th2} are material parameters, $V^{\text{eff,mode}}$ is the effective twinned fraction and $V^{\text{acc,mode}}$ is the accumulated twin fraction.

In any given grain, the twin system with the highest accumulated volume, is identified. If the highest accumulated volume fraction, for the given mode is larger than the threshold value $V^{\text{th,mode}}$ then the grain is allowed to re-orient and $V^{\text{eff,mode}}$ and $V^{\text{th,mode}}$ are both updated.

This process is repeated until either all grains are randomly checked or until the effective twin volume exceeds the accumulated twin volume (see also [45]). In the latter case reorientation by twinning is stopped and we proceed to the next deformation step.

3. IDENTIFICATION OF THE POLYCRYSTAL MODEL FOR AZ31 MG AND PREDICTIONS OF THE BEHAVIOUR FOR MONOTONIC UNIAXIAL LOADING

For calibration of the VPSC model parameters, we will use the room-temperature (25°C) stress-strain curves for quasi-static monotonic loading of AZ31 Mg (3wt%Al, 1wt%Zn, Mg bal.) rolled sheet of thickness of 2 mm reported in [2]. For each orientation, quasi-static compression specimens were prepared by bonding (using J-B Weld adhesive) two sheets.

Since in a typical polycrystal plasticity simulation, the polycrystal is represented as a discrete set of grains, in order to correctly capture the initial texture of the material it is necessary to take as input for the VPSC model the orientation of a sufficiently large number of grains with correctly determined area fractions. To this end, in this paper the entire EBSD scan (784×808 μm^2 area) was used to generate 2762 weighted orientations. The corresponding initial texture that will be used in all the simulations presented in this work is similar to that reported in [2] (see Fig. 1). Note that the material displays a strong basal texture with an almost equal fraction of grains having the c-axis slightly tilted away from the sheet normal towards +RD and –RD, respectively (around ±30°).

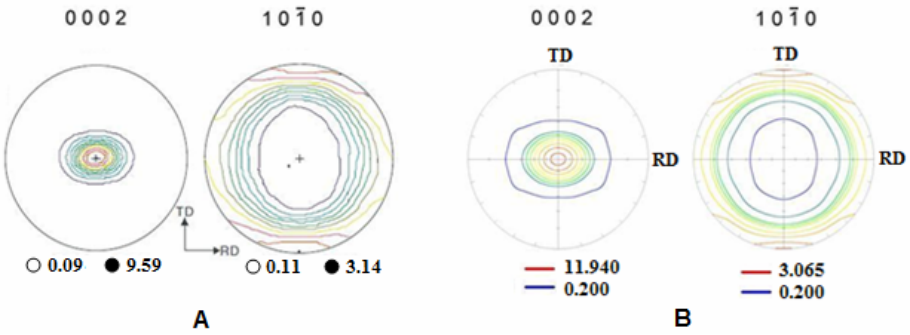

Fig. 1 – Pole figures showing initial texture of AZ31 Mg sheet: a) Reported in [2]; b) measured from a larger EBSD scan and used as input in the polycrystal model.

For calibration of the material parameters that characterize the plastic deformation at the grain level, namely the critical resolved shear stress (CRSS) and the hardening parameters associated with each deformation system that may be operational, we use a step-by-step procedure in which we isolate as much as possible the potential systems for accommodating the imposed plastic strain. We start by determining the parameters that characterize the $\{0001\}<1\bar{2}10>$ and prismatic $\{1\bar{1}00\}<11\bar{2}0>$ slip systems using the stress-strain curve in uniaxial tension along RD. The initial CRSS on all the other deformation systems is kept very high (more than six times the value of the CRSS for the prismatic slip system).

Since the initial texture is strongly basal (see Fig.1, which indicates that the c-axis of most grains is aligned with the normal direction or deviates by a very small angle from it), the activation of pyramidal $\{10\bar{1}1\}<\bar{1}\bar{1}23>$ slip system is expected in compression along the through-thickness direction of the sheet, denoted ND. Thus, the parameters associated with this system are obtained by simulating the uniaxial compression test along ND and comparing the numerical stress-strain response with the macroscopic experimental one. The parameters determined for the basal and prismatic <a> slip systems are kept fixed to the values determined based on the stress-strain curve in uniaxial tension test along RD.

A characteristic ~86° reorientation of the basal poles during uniaxial compression along RD has been observed and is attributed to the activation of the $\{10\bar{1}2\}<\bar{1}101>$ tensile twinning system. Hence, from the uniaxial compression test along RD, we identify the parameters for this extension twinning system and further estimate the validity of the identification of the $\{10\bar{1}1\}<\bar{1}\bar{1}23>$ slip system obtained based on the stress-strain curve in ND compression. The values of the parameters associated with the PTR scheme (see Eq. (5)) are: A^{th1}=0.8 and

A^{th2}=0.0 while S^t=0.145 (see Eq. (4)). Simple shear test data in RD can be used to identify the pyramidal $\{10\bar{1}1\}<\bar{1}2\bar{1}0>$ slip system (see [39]). Once those four deformation systems have been individually calibrated, the RD tension, ND compression, and RD compression tests are simulated once again in order to achieve the closest possible agreement between experimental and stress-strain response for all three loadings. For the four deformation systems, the values of the initial threshold stress τ_0^s, of the initial hardening-rate τ_1^s, the asymptotic hardening-rate θ_1^s, and the back-extrapolated threshold stress θ_0^s, which are involved in Eq. (2) are given in Table 1.

Table 1

Material parameters for the deformation systems of AZ31 Mg

System	τ_0 [MPa]	τ_1 [MPa]	θ_0	θ_1
Basal Slip: $\{0001\}<1\bar{2}10>$	17.5	5	3000	35
Prismatic Slip: $\{1\bar{1}00\}<11\bar{2}0>$	85	33	550	70
Pyramidal <a> Slip: $\{10\bar{1}1\}<\bar{1}2\bar{1}0>$	100	30	30	10
Pyramidal <c+a> Slip: $\{10\bar{1}1\}<\bar{1}\bar{1}23>$	148	50	8500	0
Tensile Twinning: $\{10\bar{1}2\}<\bar{1}101>$	52	0	0	0

In addition, self and latent hardening is modeled using the coupling coefficients $h^{ss'}$ (see Eq.(3)), which empirically account for the obstacles that new dislocations (or twins) associated with system s' create for the propagation of dislocations (or twins) on system s. For AZ31 Mg, the latent hardening coefficients $h^{ss'}$ associated with the interaction between basal and non-basal <a> slip and twinning has been set to a value of two. This reflects that low or lack of slip activity is the cause of twin formation. Given that in uniaxial compression along RD it is observed that twinning saturates at high values of strain (approx. 8%) and the slip systems are active again, the tensile twinning system must self-harden. Thus, the self-hardening parameter for tensile twinning is also set to two. On the other hand, the latent hardening coefficient $h^{ss'}$ associated with interaction between pyramidal <c+a> slip and tensile twinning is set to one in order to capture the very little twinning activity observed in ND compression.

Figure 2 shows the comparison between the predicted textures and all the experimentally available final textures for RD tension (13% strain) and RD compression (8% strain), respectively. Note that the simulated textures reproduce very well the measured textures for both loadings. Although no experimental data was available for comparison, the prediction of the texture at 6% deformation in ND compression is also given in Fig. 2c to show that the model predicts a pronounced difference between the texture obtained in ND compression and RD compression, respectively. Note the excellent agreement between model and texture data.

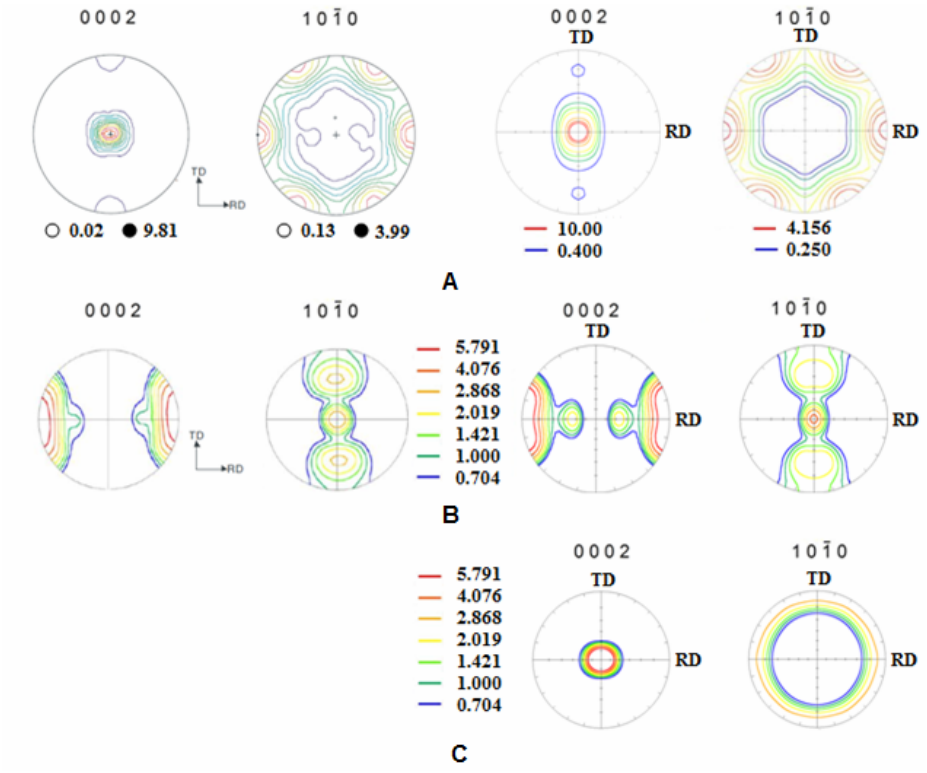

Fig. 2 – Comparison between the measured texture [2] and predicted texture: a) uniaxial tension along RD at 13% strain (~failure); b) uniaxial compression along RD at 8% strain; c) uniaxial compression along ND at 8% strain.

Although accurate predictions of the available final textures are an indication of the robustness of the calibration of the VPSC model, in the following we also verify that the mechanical response is well described, and that the predicted microstructure evolution contributing to plastic deformation corroborates. Furthermore, we check that these predictions are in agreement with general trends reported in the literature on AZ31 Mg sheets.

For RD tension comparison between the VPSC model predictions of the stress-strain response and data is shown in Fig. 3. On the same figure is shown the predicted texture evolution at 6% strain and 12% strain, respectively. Note that the experimental stress-strain response (symbols) is well reproduced by the model (solid line). The predicted RD tension curve exhibits a decreasing work hardening rate, which also indicates that the plastic deformation is dominated by slip.

The predicted mechanical response and predicted textures at 6% strain and 12% strain in RD compression are shown in Fig. 4. Note that the predicted (0002) pole figures show a marked evolution of texture because basal slip and extension twinning are the dominant modes of deformation for this strain path and their relative activity gives the characteristic ~86° rotation of the basal plane which has also been observed in the mechanical test sample at 8% strain in RD compression (Fig. 2). The interaction between twinning and slip systems also explains the peculiar changes in work-hardening (the knee between ~3% and 5% strain) and the concave-up appearance of the stress-strain curve above 6% strain). Both those unusual features of the hardening of the material under RD compression are well captured by the model.

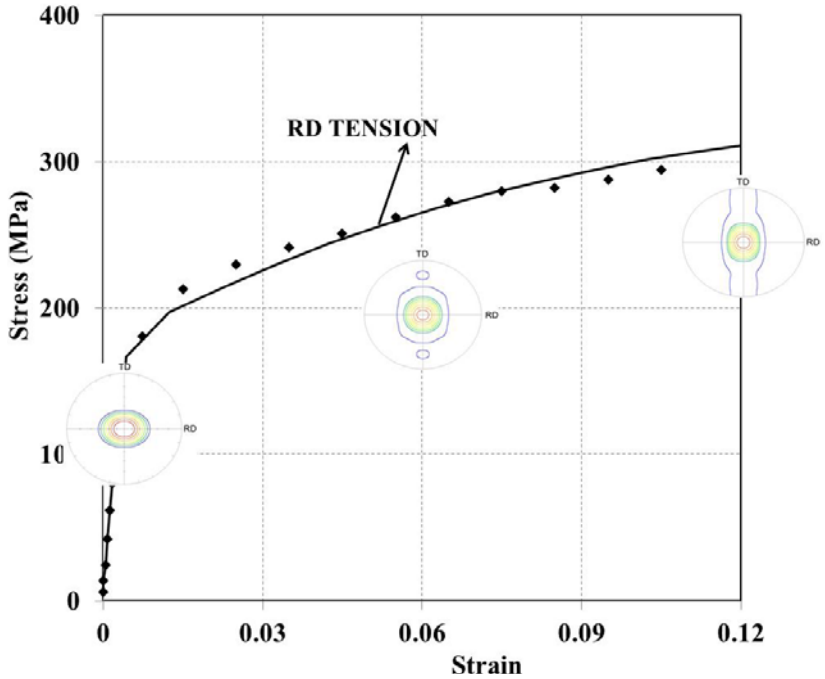

Fig. 3 – Stress-strain response and evolution of the microstructure according to the VPSC model calibrated using the outlined procedure in comparison with mechanical test data (symbol) in RD tension.

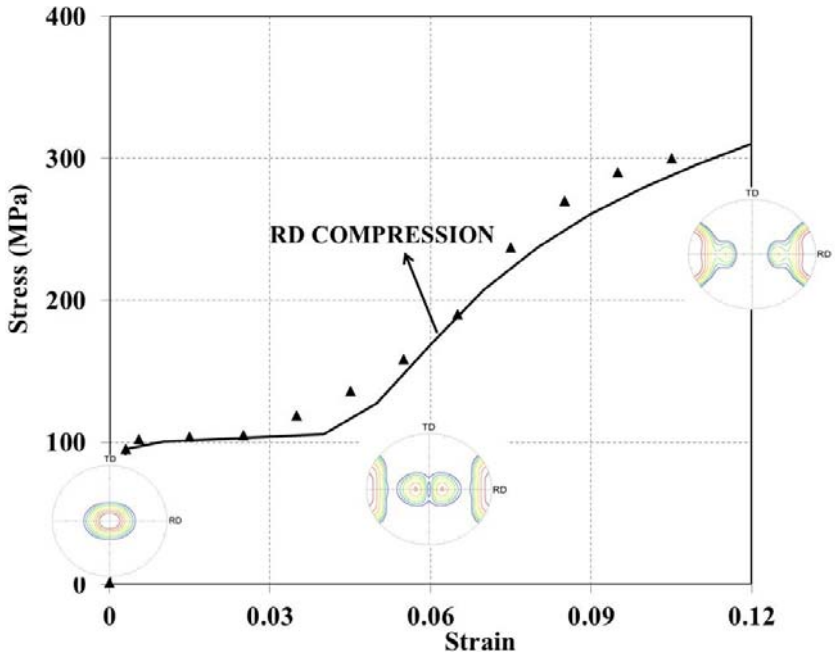

Fig. 4 – Stress-strain response and evolution of the microstructure according to the VPSC model calibrated using the outlined procedure in comparison with mechanical test data (symbol) in RD compression.

Figure 5 shows the stress-strain response obtained from the ND compression test (symbols) and the predictions of the VPSC model (lines) along with, the predicted evolution of texture. From the predicted basal pole figures, it can be seen that as the plastic strain increases, the c-axis of the majority of grains further aligns with the sheet normal. Thus, the observed changes in microstructure can be attributed mainly to crystallographic slip activities.

Although the predominant twinning reorientation (PTR) model represents a simplified scheme for treating twinning compared to other models (e.g. the composite grain model [30]) and the hardening law (Eq. (2) is much simpler than those proposed in [46], both the stress-strain response and texture evolution are captured well.

Next, the polycrystalline model is used to predict the material's mechanical response for monotonic strain paths that were not considered in the model calibration. We simulate the material behavior for uniaxial tension and compression along TD (in-plane direction at 90° from RD). In these simulations we use the same values of the material parameters (i.e. the values of the parameters given in Table 1). In each simulation, initially all the systems are considered active. Fig. 6 shows the stress-strain response obtained from the mechanical test (symbols) and the predictions of the model (lines) in TD tension, along with, the predicted textures at 6% strain and 12% strain, respectively.

In TD tension, the plastic deformation is completely accommodated by slip; the predicted texture evolution suggests rapid alignment of the grains such that the basal planes lie parallel to the sheet surface along the loading direction (i.e. TD). Note also that the intensity contours in TD tension are rotated at 90° to those in RD tension (compare Fig. 3 and Fig. 6, respectively).

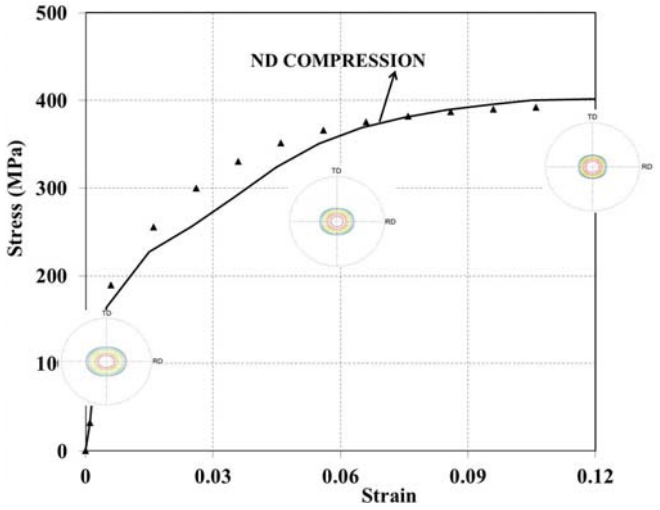

Fig. 5 – Stress-strain response and evolution of the microstructure according to the VPSC model calibrated using the outlined procedure in comparison with mechanical test data (symbol) in ND compression.

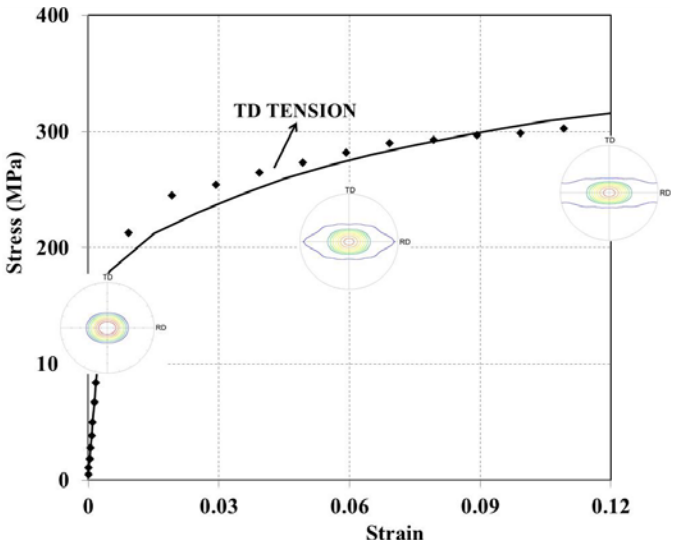

Fig. 6 – Stress-strain response and evolution of the microstructure according to the VPSC model calibrated using the outlined procedure in comparison with mechanical test data (symbol) in TD tension.

Figure 7 shows the experimental stress-strain response in comparison with the predictions of the VPSC model in TD compression, along with the predicted textures at 6% strain and 12% strain, respectively. The agreement between the model predictions of the stress-strain response and data is excellent. No texture measurements were available for comparison. Nevertheless, analysis of predicted textures shows that at higher strains the c-axis of the majority of grains is rotating towards the transverse direction and becomes aligned with TD.

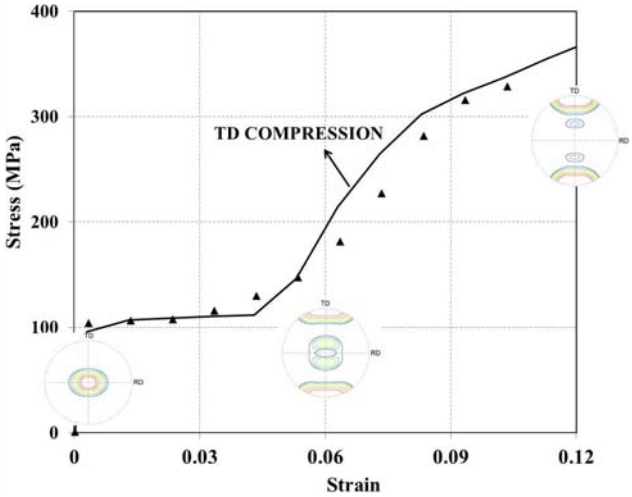

Fig. 7 – Stress-strain response and evolution of the microstructure according to the VPSC model calibrated using the outlined procedure in comparison with mechanical test data (symbol) in TD compression.

4. PREDICTIONS OF THE POLYCRYSTAL MODEL FOR CHANGING STRAIN PATHS

It is investigated whether using the same set of values for the parameters (CRSS and hardening parameters) of all the slip and twin systems, it is possible to predict the mechanical response of a thinner rolled AZ31 sheet (0.8 mm thickness) with similar initial texture for which room-temperature monotonic and cyclic tests were reported by Hama and collaborators (see [25–26]). For the thinner AZ31 sheet, the parameters S^t (see Eq. (4)), A^{th1} and A^{th2} used in the PTR scheme were slightly modified because the initiation and saturation of twinning in monotonic RD compression were slightly different. Those values are: $A^{th1}=0.7$, $A^{th2}=0.7$, and $S^t=0.105$.

Figure 8 shows the predicted and measured stress-strain response for monotonic loadings reported in [25].

As mentioned, in [25] and [26] stress-strain curves obtained in cyclic tests starting with tension or compression were also reported. Since the focus of our

investigation is on addressing the effect of strain-path changes on the stress-strain response and the microstructure, we analyse tension-compression-tension (T-C-T) behaviour, and respectively compression-tension-compression (C-T-C) behaviour. Consequently, we compare our simulation results with the respective stress-strain response reported in Hama *et al*. [25–26] for the first T-C-T and C-T-C cycle of the tests, respectively.

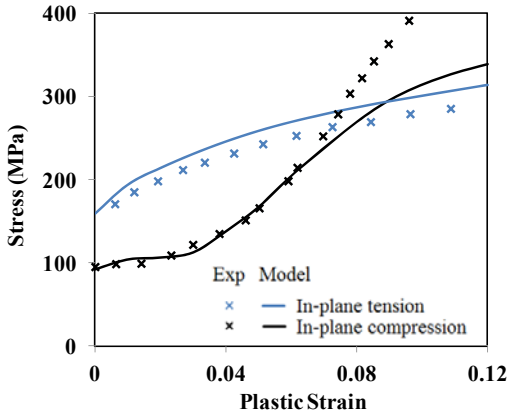

Fig. 8 – Comparison between experimental data from [25] (symbol) and VPSC model prediction (line) for uniaxial in-plane tension and in-plane compression tests.

We begin by simulating the mechanical response in tension-compression-tension observed in a cyclic test with strain amplitude of 4%. The imposed strain path consisted of uniaxial tension up to 2% strain (point A in Fig. 9) followed by partial unloading to 1% strain (point B in Fig. 9) then loading in compression to –2% strain (point D in Fig.9), then unloading, and reloading in tension (yielding in tension occurring at point E, see Fig. 9) up to 2% strain.

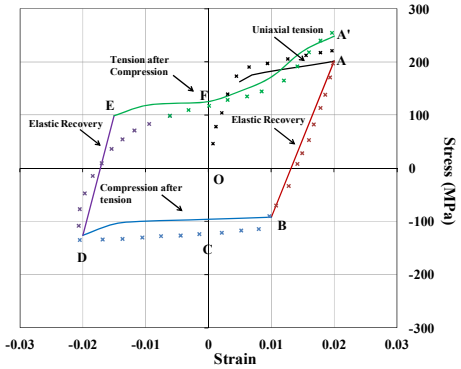

Fig. 9 – Comparison of the stress-strain response measured by [25] (symbol) against that predicted by VPSC model (lines) for AZ31 Mg material subjected to a tension-compression-tension test with 4% strain amplitude and no pre-strain.

First, let us note that the VPSC model correctly predicts the stress-strain response in this test.

The simulations also show that under uniaxial tension, the initial texture is rotated such that the basal planes tend to align themselves along RD. Note also that there is no rotation of the c-axes of the grains. The predicted texture corresponding to 2% strain (point A) is shown in Fig. 10a. Unloading is considered elastic, with slope equal to the experimental Young modulus (~40 GPa, based on [25]), so the texture at points A and point B are the same. During subsequent compression loading, the model predicts no texture evolution (compare textures at point A and point C), and almost constant hardening rate until tensile twinning activates (between points B and D) producing the typical kink in the stress-strain curve (sigmoidal shape). The texture at –2% strain (point D, see Fig. 10c) also indicates that the c-axes of some of the grains are aligned with the compression direction (RD). Note that in the early stages of loading in tension following compression (i.e. up to point F, see Fig. 10d), the model predicts no significant change in texture, the deformation being accommodated by slip. However, with increasing strain, tensile twinning is activated, thus inducing further rotation of the c-axes and the texture at 2% strain (point A') becomes basal (see Fig. 10e).

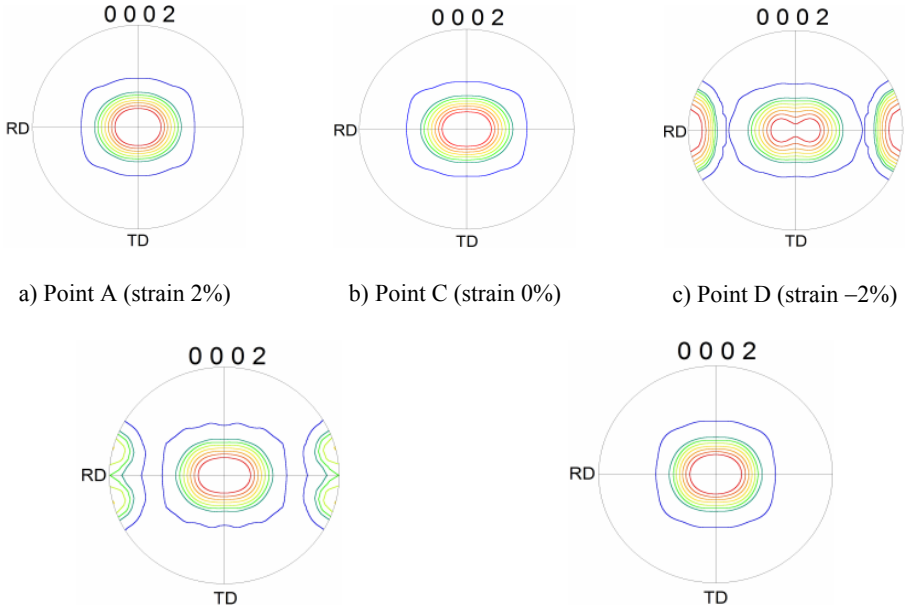

a) Point A (strain 2%) b) Point C (strain 0%) c) Point D (strain –2%)

d) Point F (strain 0%) e) Point A' (strain 2%)

Fig. 10 – Predicted texture evolution in a tension-compression-tension (T-C-T) test with 4% strain amplitude and no pre-strain: a) texture at point A; b) point C; c) point D; d) point F; e) point A'.

Figure 11 shows the predicted stress-strain response in a cyclic test with strain amplitude of 6% in comparison with the experimental data reported in [25].

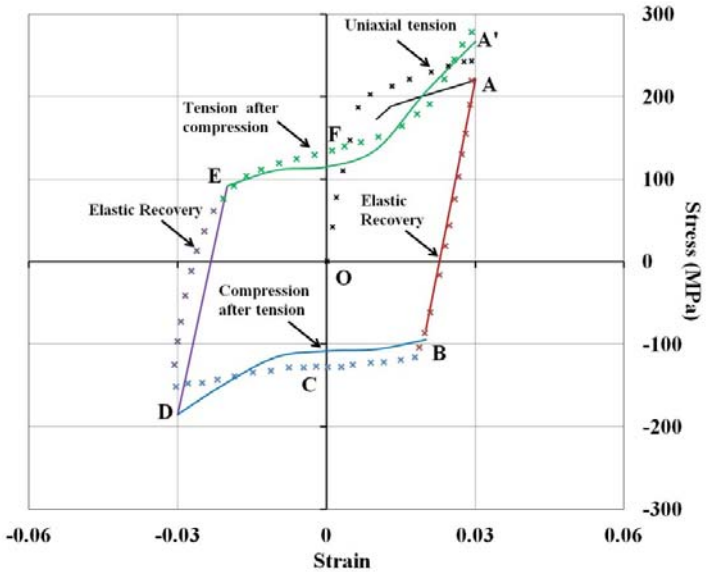

Fig. 11 – Comparison of stress-strain response measured by [25] (symbol) against that predicted by VPSC model (lines) for AZ31 Mg material subjected to a tension-compression-tension (T-C-T) test with 6% strain amplitude and no pre-strain.

Note that if the material is subjected to the same loading path, but at higher strain amplitude, the sigmoidal shape displayed in compression following tension is more pronounced. Also, more grains have their c-axes oriented along RD as it can be clearly seen by comparing the predicted texture at –2% shown in Fig 10b with the predicted texture at –3% shown in Fig. 12c. Likewise, under uniaxial tension following compression the amount of twinning is larger as compared to the test at lower amplitude. Nevertheless, irrespective of the strain amplitude, the model predicts that a basal texture is recovered.

It is to be noted that in [25] no texture measurements were reported, so no direct comparison with the predicted textures could be made. However, in [25] are given the photographs of the microstructures corresponding to the points A (strain of 3%), B (strain of 1.5%), C (strain of –0.75%), D (strain of –3%), E (strain of –1.5%), F (strain of 0.75%) and A' (strain of 3%) of Fig. 11. Comparison between the initial microstructure and that at point A (i.e. after 3% loading in tension) indicates that the deformation is accommodated mainly by slip, as predicted by the model (see predicted texture at point A shown in Fig. 12a). The data presented indicates that unloading does not affect the microstructure, so the hypothesis of elastic unloading is valid.

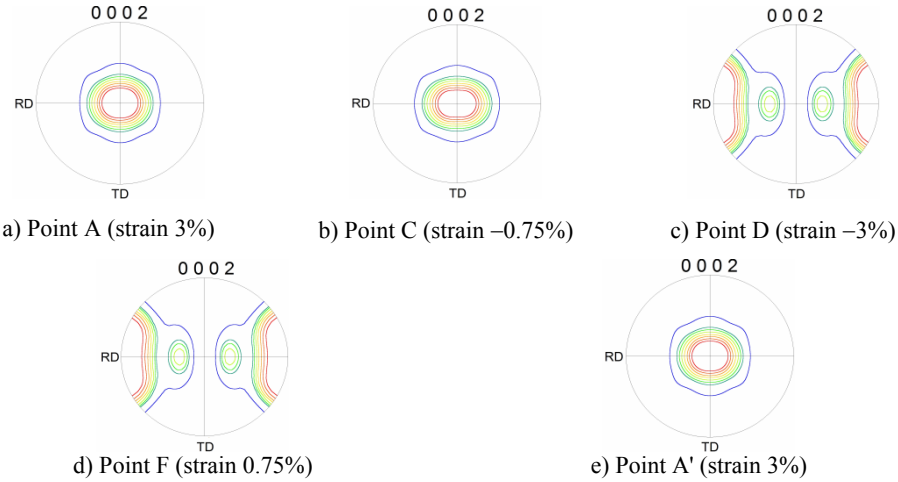

a) Point A (strain 3%) b) Point C (strain –0.75%) c) Point D (strain –3%)

d) Point F (strain 0.75%) e) Point A' (strain 3%)

Fig. 12 – Predicted texture evolution in a tension-compression-tension (T-C-T) test with 6% strain amplitude and no pre-strain: a) texture at point A; b) point C; c) point D; d) point F; e) point A'.

The microstructure at point D, i.e. at the end of the compression stage, reported in [25] shows significant deformation twinning, which corroborates with the predicted texture at D, shown in Fig. 12c (namely, rotation of the c-axes of most grains). The microstructure at point A', i.e. at the end of the T-C-T cycle, shows that the initial microstructure is recovered. This corroborates with the predicted texture at A' (see Fig. 12e).

Next, we examine whether the model can predict the influence of pre-strain on the work-hardening response of the material under cyclic tension-compression loadings along RD. The simulation results are compared with the experimental stress-strain curves reported in [26].

Figure 13a shows the results obtained in a cyclic test with strain amplitude of 4% and a tensile pre-strain of 4%. The agreement between simulations and data is very good. Most importantly, comparison between the results for the same amplitude and 0% pre-strain (Fig. 9) and the results when the tensile pre-strain was applied (Fig. 13(a)) show that the overall tendencies remain the same. With or without tensile pre-strain, under tension loading followed by compression, and further tension (i.e. T-C-T), the material shows an increase in the rate of hardening during the second tensile loading, the stress-strain curve displaying a sigmoidal shape. On the other hand, both the simulation and experimental results obtained in a cyclic test consisting of compression followed by tension (C-T-C) with the same strain amplitude of 4% show that in tension after compression the stress-strain curve does not have a sigmoidal shape (see Fig. 13b). However, the influence of amount of pre-strain in compression is very important. In a C-T-C test with compressive pre-strain of 2%, the rate of hardening in the tension stage is much higher than in the case when the pre-strain is larger, as evidenced by comparing the

results shown in Fig 3c (compressive pre-strain of 2%) with those in Fig. 13b (compressive pre-strain of 4%). This can be explained based on the texture evolution in RD compression predicted by the model. Indeed, in the CTC test shown in Fig. 13b, the tension stage followed a compressive loading to 6% while in the CTC test shown in Fig. 13c, the tension stage followed compression only to 4%. Comparison between the textures after 6% compression and that corresponding to 4% RD compression shows that in the latter much fewer grains have their c-axes reoriented than in the former case (see Fig. 14 showing the predicted texture evolution during RD compression). Hence, the predicted difference in hardening behaviour in tension following 4% compression, and –6% compression, respectively. Simulations of the behaviour in CTC and respectively TCT tests with amplitude of 6% and pre-strains of 4%, –2%, –4% are shown in Fig. 15. The agreement between model and data is also very good.

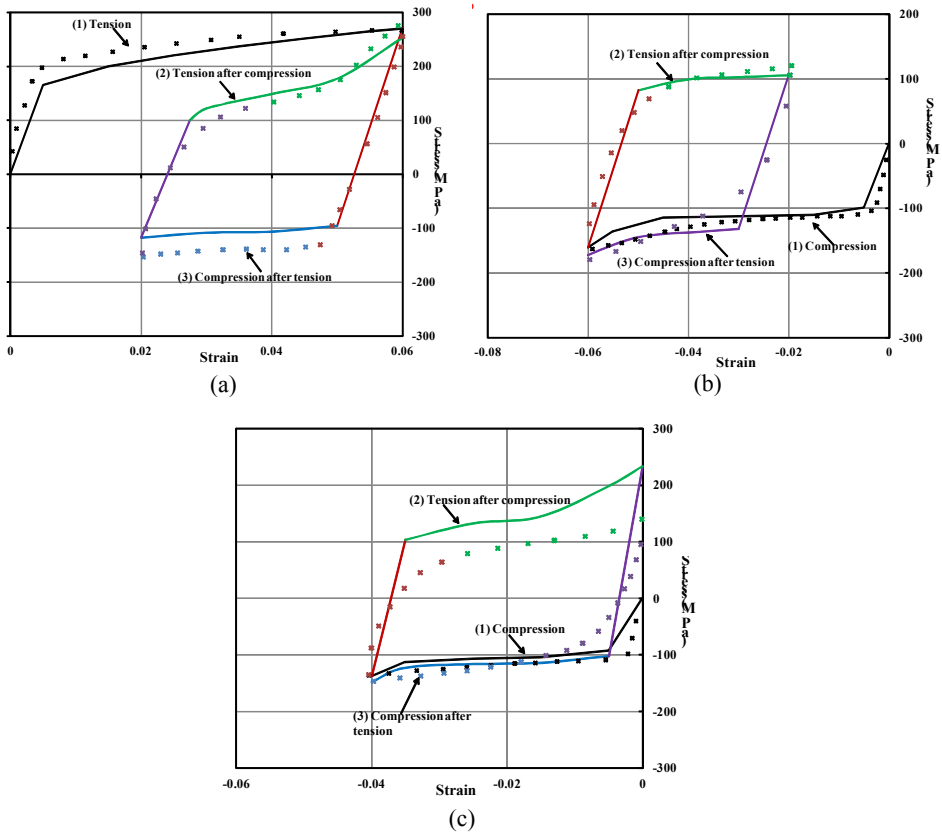

Fig. 13 – Comparison of stress-strain response measured by [26] (symbol) against that predicted by VPSC model (lines) for AZ31 Mg material subjected to tests with strain amplitude of 4% : a) tension-compression-tension (T-C-T) with pre-strain of 4%; b) compression-tension-compression (C-T-C) with pre-strain of –4%; c) compression-tension-compression (C-T-C) with pre-strain of –2%.

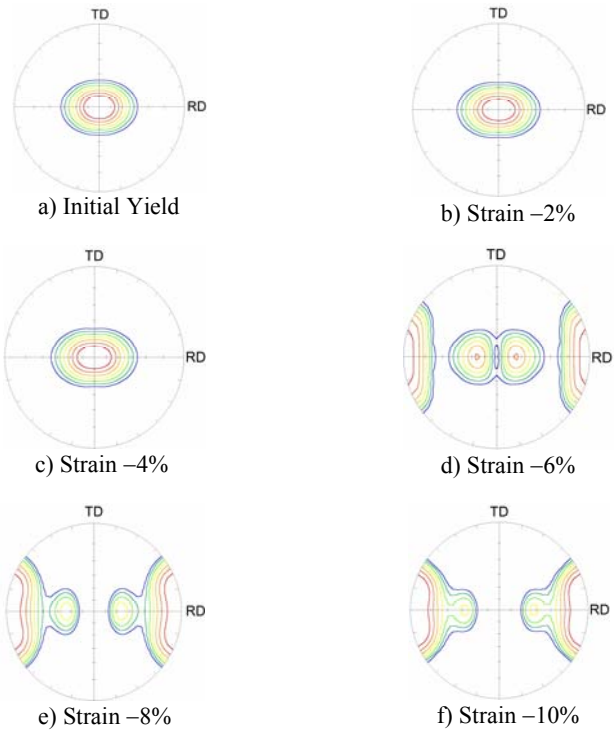

a) Initial Yield b) Strain –2%

c) Strain –4% d) Strain –6%

e) Strain –8% f) Strain –10%

Fig. 14 – Predicted texture evolution in a monotonic RD compression test at strain: a) 0%; b) –2%; c) –4%; d) –6%; e) –8%; f) –10%.

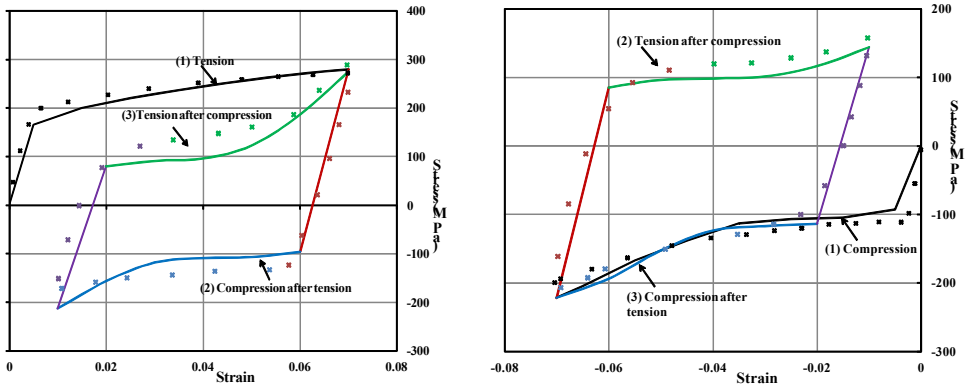

a) b)

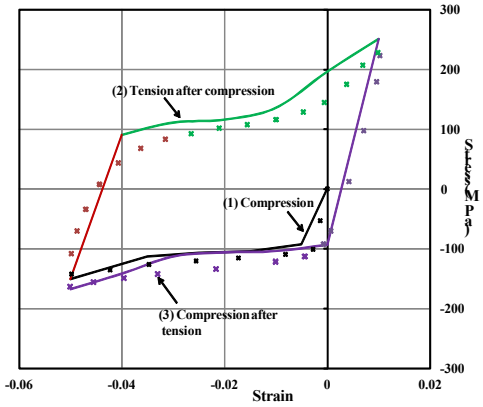

c)

Fig. 15 – Comparison of stress-strain response measured by [26] (symbol) against that predicted by VPSC model (lines) for AZ31 Mg material subjected to tests with strain amplitude of 6% : a) tension-compression-tension (T-C-T) test with pre-strain of 4%; b) compression-tension-compression (C-T-C) test with pre-strain of –4%; c) compression-tension-compression (C-T-C) test with pre-strain of –2%.

5. CONCLUSION

In this paper, a step-by-step approach for the calibration of the VPSC model for AZ31 Mg was presented. Using this procedure all the material parameters were identified from a few simple monotonic tests. Specifically, it was shown that by accounting for the deformation mechanisms active in the microstructure during loading for one uniaxial tension test (along RD) and two compression tests (along RD and ND), it is possible to explain, and accurately predict the stress-strain behavior and texture evolution under monotonic uniaxial loading for all orientations.

It was also investigated whether with the same set for all the slip and twin systems, it is possible to predict the mechanical response of a thinner rolled AZ31 sheet (0.8 mm thickness) with similar initial texture for which room-temperature monotonic and cyclic tests were reported in [25–26]. It was shown that if the slip and twinning activity in uniaxial loadings is properly identified with the simple PTR scheme for twinning re-orientation, it is possible to describe the difference in behavior in terms of stress-strain response between tension-compression-tension and compression-tension-compression loadings.

Since no texture measurements were given, a direct comparison of predicted and measured textures could not be made. However, partial verification of the overall trends in terms of microstructure evolution was done based on the photographs of the experimental microstructures.

The following conclusions can be drawn from the predicted texture evolution:

- With or without tensile pre-strain, under tension loading followed by compression, and further tension (i.e. T-C-T loading), the material shows an increase in the rate of hardening during the second tensile loading, the stress-strain curve displaying a sigmoidal shape.
- On the other hand, both the simulation and experimental results obtained in a cyclic test consisting of compression followed by tension (C-T-C) with the same strain amplitude show that in tension after compression the stress-strain curve may or may not have a sigmoidal shape. In this case, the influence of amount of pre-strain in compression is very important.

Acknowledgements. Partial support for this work provided by the AFRL Mathematical and Optimization Institute is gratefully acknowledged. The authors would also like to thank Dr. Ricardo Lebensohn of Los Alamos National Laboratory for fruitful discussions and providing the VPSC code.

Received on June 24, 2015

REFERENCES

1. KELLEY, E.W., HOSFORD, W., *The deformation characteristics of textured magnesium*, Trans Met Soc AIME, **242**, *4*, pp. 5–13, 1968.
2. KHAN, A., PANDEY, A., GNAUPEL-HEROLD, T., MISHRA, R.K., *Mechanical response and texture evolution of AZ31 alloy at large strains for different strain rates and temperatures*, Int. J. Plast., **27**, *5*, pp. 688–706, 2011.
3. LOU, X.Y., LI, M., BOGER, R.K., AGNEW, S.R., WAGONER, R.H., *Hardening evolution of AZ31B Mg sheet*, Int. J. Plast., **23**, *1*, pp. 44–86, 2007.
4. AGNEW, S.R., DUYGULU, O., *Plastic Anisotropy and the role of non-basal slip in magnesium alloy AZ31B*, Int. J. Plast., **21**, *6*, pp. 1161–1193, 2005.
5. MEKONEN, M.N., STEGLICH D., BOHLEN J., LETZIG D., MOSLER J., *Mechanical characterization and constitutive modeling of Mg alloy sheets*, Mat. Sci. Eng. A, **540**, pp. 174–186, 2012.
6. BEAUSIR, B., TOTH, L.S., QODS, F., NEALE, K.W., *Texture and mechanical behavior of Magnesium during free-end torsion*, J. Eng. Mat. Technol., **131**, *1*, pp. 1–15, 2008.
7. BISWAS, S., BEAUSIR, B., TOTH, L. S., SUWAS, S., *Evolution of texture and microstructure during hot torsion of a magnesium alloy*, Acta Mat., **61**, *14*, pp. 5263–5277, 2013.
8. GUO, X.Q.,WU, W., WU, P.D., QIAO, H., AN K., LIAW P.K., *On the Swift effect and twinning in a rolled magnesium alloy under free-end torsion*, Scripta Mater., **69**, *4*, pp. 319–322, 2013.
9. SCUTTI, J. J., *Flowformed titanium tubular products*, Adv. Mat. Processes, **159**, pp. 69–70, 2001.
10. HILL, R., *A theory of the yielding and plastic flow of anisotropic metals*, Proceedings of the Royal Society of London A: Math., Phy. and Eng. Sci., **193**, *1033*, pp. 281–297, 1948.
11. BARLAT, F., LEGE, D.J., BREM, J.C., *A six-component yield function for anisotropic materials*, Int. J. Plast., **7**, *7*, pp. 693–712, 1991.
12. BARLAT, F., MAEDA, Y., CHUNG, K., YANAGAWA, M., BREM, J.C., HAYASHIDA, Y., MAKOSEY, S., *Yield function development for aluminum alloy sheets*, J. Mech. Phy. of Solids, **45**, *11–12*, pp. 1727–1763, 1997.

13. BARLAT, F., YOON, J.W., CAZACU, O., *On linear transformations of stress tensors for the description of plastic anisotropy*, Int. J. Plast., **23**, *5*, pp. 876–896, 2007.
14. CAZACU, O., BARLAT, F., *Generalization of Drucker's yield criterion to orthotropy*, Math. Mech. of Solids, **6**, *6*, pp. 613–630, 2001.
15. CAZACU, O., BARLAT, F., *A criterion for description of anisotropy and yield differential effects in pressure-insensitive metals*, Int. J. Plast., **20**, *11*, pp. 2027–2045, 2004.
16. CAZACU, O., PLUNKETT, B., BARLAT, F., *Orthotropic yield criterion for hexagonal closed packed materials*, Int. J. Plasticity, **22**, *7*, pp. 1171–1194, 2006.
17. NIXON, M.E., CAZACU, O., LEBENSOHN, R.A., *Anisotropic response of high-purity α-titanium: Experimental characterization and constitutive modeling*, Int. J. Plasticity, **26**, *4*, pp. 516–532, 2010.
18. GRAFF, S., BROCKS, W., STEGLICH, D., *Yielding of magnesium: from single crystal to polycrystalline aggregates*, Int. J. Plast., **23**, *12*, pp. 1957–1978, 2007.
19. CAZACU, O., REVIL-BAUDARD, B., BARLAT, F., *New interpretation of monotonic Swift effects: Role of tension–compression asymmetry*, Mech. of Materials, **57**, pp. 42–52, 2013.
20. CAZACU, O., REVIL-BAUDARD, B., BARLAT, F., *New interpretation of cyclic Swift effects*, Euro. J. Mechanics-A/Solids, **44**, pp. 82–90, 2014.
21. REVIL-BAUDARD, B., CHANDOLA, N., CAZACU, O., BARLAT, F., *Correlation between swift effects and tension–compression asymmetry in various polycrystalline materials*, J. Mech. Phy. of Solids, **70**, pp. 104–115, 2014.
22. CHANDOLA, N., LEBENSOHN, R.A., CAZACU, O., REVIL-BAUDARD, B., MISHRA, R.K., BARLAT, F., *Combined effects of anisotropy and tension–compression asymmetry on the torsional response of AZ31 Mg*, Int. J. of Solids and Struct., **58**, 190–200, 2015.
23. LI, M., LOU, X.Y., KIM, J.H., WAGONER, R.H., *An efficient constitutive model for room temperature, low-rate plasticity of annealed Mg AZ31B sheet*, Int. J. Plast., **26**, *6*, pp. 820–858, 2010.
24. WANG, H., WU, P. D., WANG, J., TOMÉ, C.N., *A crystal plasticity model for hexagonal close packed (HCP) crystals including twinning and de-twinning mechanisms*, Int. J. of Plast., **49**, 36–52, 2013.
25. HAMA, T., KARIYAZAKI, Y., HOSOKAWA, N., FUJIMOTO, H., TAKUDA, H., *Work-hardening behaviors of magnesium alloy sheet during in-plane cyclic loading*, Mat. Sci. Eng. A, **551**, pp 209–217, 2012.
26. HAMA, T., NAGAO, H., KUCHINOMACHI, Y., TAKUDA, H., *Effect of pre-strain on work-hardening behavior of magnesium alloy sheets upon cyclic loading*, Mat. Sci. Eng. A, **591**, pp. 69–77, 2014.
27. VAN HOUTTE, P., *Simulation of the rolling and shear texture of brass by the Taylor theory adapted for mechanical twinning*, Acta Metall., **26**, *4*, pp. 591–604, 1978.
28. TOMÉ, C.N., LEBENSOHN, R., KOCKS, U.F., *A model for texture development dominated by deformation twinning: application to Zirconium alloys*, Acta Metall. et Mat., **39**, *11*, pp. 2667–2680, 1991.
29. WU, X., KALIDINDI, S.R., NECKER, C., SALEM, A.A., *Prediction of crystallographic texture evolution and anisotropic stress-strain curves during large plastic strains in high purity α-Titanium using a Taylor-Type crystal plasticity model*, Acta Mater., **55**, *2*, pp. 423–432, 2007.
30. PROUST, G., TOMÉ, C.N., JAIN, A., AGNEW, S.R., *Modeling the effect of twinning and detwinning during strain-path changes of magnesium alloy AZ31*, Int. J. Plast., **25**, *5*, pp. 861–880, 2009.
31. TAYLOR, G.I., *Plastic strain in metals*, J. of the Institute of Metals, **62**, pp. 307–324, 1938.
32. TAYLOR, G.I., *Analysis of plastic strain in a cubic crystal*, in: *Stephen Timoshenko 60th Anniversary*, Mcmillan Co., New York, 1938, pp. 218–224.
33. LEBENSOHN, R.A., TOMÉ, C.N., *A self-consistent anisotropic approach for the simulation of plastic deformation and texture development of polycrystals: Application to zirconium alloys*, Acta Metall. et Mater., **41**, *9*, pp. 2611–2624, 1993.

34. WANG, H., WU, P.D., TOMÉ, C.N., HUANG, Y., *A finite strain elastic-viscoplastic self-consistent model for polycrystalline materials*, Journal of the Mechanics and Physics of Solids, **58**, *4*, pp. 594–612, 2010.
35. JAIN, A., AGNEW, S.R., *Modeling the temperature dependent effect of twinning on the behavior of magnesium alloy AZ31B sheet*, Mat. Sci. Eng. A, **462**, pp. 29–36, 2007.
36. CHOI, S.H., KIM, D.H., SEONG, B.S., *Simulation of strain-softening behaviors in an AZ31 Mg alloy showing distinct twin-induced reorientation before a peak stress*, Metals Mater. Int., **15**, pp. 239–248, 2009.
37. WANG, H., RAEISINIA, B., WU, P.D., AGNEW S.R., TOMÉ, C.N., *Evaluation of self-consistent polycrystal plasticity models for magnesium alloy AZ31B sheet*, Int. J. of Solids and Struct., **47**, *21*, pp. 2905–2917, 2010.
38. WALDE, T., RIEDEL, H., *Simulation of earring during deep drawing of magnesium alloy AZ31*, Acta Mater., **55**, *3*, pp. 867–874, 2007.
39. CHANDOLA, N., MISHRA, R.K., CAZACU, O., *Application of the VPSC model to the description of the stress-strain response and texture evolution in AZ31 Mg for various strain paths*, Eng. Mater. Tech., In-press, 2015.
40. LEBENSOHN, R., *Modelling the role of local correlations in polycrystal plasticity using viscoplastic self-consistent schemes*, Model. Sim. Mat. Sci. Eng., **7**, *5*, pp. 739–746, 1999.
41. TOMÉ, C.N., KASCHNER, G.C., *Modeling texture, twinning and hardening evolution during deformation of hexagonal materials*, Materials Science Forum, **495**, pp. 1001–1006, 2005.
42. PROUST, G., TOMÉ, C.N., KASCHNER, G.C., *Modeling texture, twinning and hardening evolution during deformation of hexagonal materials*, Acta Mat., **55**, *6*, pp. 2137–2148, 2007.
43. HAMA, T., KITAMURA, N., TAKUDA, H., *Effect of twinning and detwinning on inelastic behavior during unloading in a magnesium alloy sheet*, Mat. Sci. Eng. A, **583**, pp. 232–241, 2013.
44. TOMÉ, C.N., LEBENSOHN, R.A., *Self consistent homogenization methods for texture and anisotropy* (Chap. 23) in: *Continuum Scale Simulation of Engineering Materials: Fundamentals-Microstructures-Process Applications* (eds. D. Raabe, F. Roters, F. Barlat, L.-Q. Chen), 2004, pp. 473–499.
45. TOMÉ, C.N., LEBENSOHN, R.A., *Manual for code viscoplastic self-consistent* (Version 7), Available at: http://public.lanl.gov/vpsc, 2008.
46. BEYERLEIN I.J, TOMÉ C.N, *A dislocation-based constitutive law for pure Zr including temperature effects*, Int. J. Plast., **24**, *5*, pp. 867–895, 2008.